Organic Photonics and Photovoltaics
Research Article • DOI: 10.2478/oph-2013-0002 • OPP • 2013 • 11-23

VERSITA

# Continuous lateral gradients in film morphology for position sensitive detection and organic solar cell optimization

**Abstract**

We present a method to fabricate binary organic donor and acceptor blends exhibiting a controlled lateral gradient in morphology. Upon combining photometry, ellipsometry and X-ray maps together with photoinduced absorption measurements, we show how the gradual exposure to solvent vapor results in a varying degree of polymer crystallinity for the polythiophene/soluble fullerene system along one direction. These morphologically graded samples are characterized by a spectral photoresponse that depends on the specific location in the area of the device where the light beam impinges, a property that stands as proof-of-concept for position sensitive detection. Moreover, we demonstrate that the development of graded morphologies is an effective one-step method which allows for fast performance optimization of organic solar cells. Finally, the appropriateness of eight different solvents for morphology control via vapor annealing is evaluated in a time-effective way using the advanced method, which helps to identify boiling point and solubility as the key processing parameters.

**Keywords**

organic photovoltaics • position sensitive detectors • combinatorial screening • morphology gradients

PACS: 02.10.Ox; 85.60.-q; 81.05.Fb; 61.66.Hq; 88.40.jr



M. Campoy-Quiles[1]*, V. Randon[1], M. M. Mróz[2], M. Jarzaguet[1], M. Garriga[1], J. Cabanillas-González[2]

1 *Institut de Ciència de Materials de Barcelona (ICMAB-CSIC), Esfera UAB, Bellaterra 08193, Spain*

2 *Instituto Madrileño de Estudios Avanzados en Nanociencia (IMDEA-Nanociencia), Cantoblanco, 28049 – Madrid, Spain*

Received 2/21/2013
Accepted 4/15/2013

## 1. Introduction

Organic solar cells (OSC) and photodetectors show great potential as low cost and easy processing photovoltaic technologies. Their operation relies on an efficient photoinduced charge transfer between electron donor (*p*-type) and electron acceptor (*n*-type) materials. Conventional device geometries include either planar heterojunctions (e.g. bilayer structures, often fabricated by evaporation of small molecular species) or bulk heterojunctions (BHJ), in which a fine mixing of the two components is achieved either by co-processing in solution or co-evaporation. Controlling the morphology of organic photovoltaic blends at the micro and nano scale is one of the key parameters when optimizing organic photovoltaics efficiency. For instance, the morphological changes induced by thermal annealing have achieved more than a two-fold increase in OSC power conversion efficiency [1–3] and four orders of magnitude reduction in photodetector dark current [4]. This fact has encouraged the search for processing protocols in which the resulting morphology is optimal for photovoltaic operation. For BHJ OSC, this morphology consist of a bicontinuous mixture of donor and acceptor molecules with domains sizes of some tens of nanometers. The optimum size constitutes a compromise between large domains, where percolation is assured and improved charge collection is obtained (reduced bimolecular recombination), and small domains where larger interfacial area-to-volume ratio leads to a high probability of photoinduced charge transfer.

Typically, the optimization procedure consists of fabricating a series of samples in which one parameter is explored. For instance, preparing samples annealed at different temperatures [1, 3, 5], during different vapor annealing times [6, 7], during different drying times [8] or includ-

*E-mail: mcampoy@icmab.es

ing variable amounts of a given additive [9]. Optimization may then, involve fabrication and testing of a large number of samples. Lateral homogeneity throughout the area of each individual sample is always fundamental in order to consider successful a given processing protocol [10].

Here we introduce an alternative route for optimization of organic photovoltaics inspired by combinatorial screening techniques, where gradients in morphology are created within a single sample by gradually exposing local zones within the device active area to different solvent annealing conditions. This allows exploring the annealing parameter space in a time effective manner and with a high degree of accuracy. The proposed methodology involves the fabrication of a small number of devices with a controlled lateral structural gradient whereas conventional multi-sample screening would otherwise require the development of a large number of homogeneous samples. The advanced concept and methodology could be of great interest for efficient screening of novel OSC materials.

As the photovoltaic spectral response will gradually vary depending on the local structure, this type of graded devices could, on the other hand, be of potential interest as position sensitive detectors (PSD). PSDs are a type of devices that allows detecting the specific place where light hits the surface of the detector [11–16]. PSDs have multiple applications from telecommunications (laser alignment) to robotics (following the movement of objects) passing through medical imaging. Lateral PSDs are based on a single pixel configuration comprising one or more resistive layers. These devices are able to monitor the position of light on the active layer with good accuracy over small distances. Their resistive nature implies, however, a limitation for position monitoring over large distances. PSDs based on arrays of pixels with resolution limited by effective pixel size can also be developed for large distance position monitoring although they require more complicated electronics to drive them and their complexity and cost increases significantly with the array size. The here introduced concept implies a single pixel device with an active layer morphology which varies along one direction. In contrast to lateral PSDs, the principle of operation is based on charge collection perpendicular to the contact (through the film thickness) rather than being based on the variations in lateral resistivity. Therefore no size limitations are expected with this device layout. As only one pixel is needed, the organic PSD based on morphology gradients can achieve high resolution over large sizes without requiring complex electronics [14, 16]. We have already shown in a previous publication how the spectral response of small molecule multilayer photodetectors can be spatially tuned by implementing wedge-shaped active layers [15]. In that case, the strong dependence of the in-depth light distribution with film thickness was exploited for determining the position of the impinging light on the active area with a resolution better than 600 µm [16].

Here we produce organic PSDs based on morphology rather than thickness gradients, thus extending the concept to devices fabricated by easily implemented solution based processing. First we show a method to create controlled lateral gradients in morphology for bulk heterojunctions comprising poly(3-hexylthiophene) (P3HT) mixed with [6,6]-phenyl C61-butyric acid methyl ester (PCBM). The method is based on gradually introducing the sample on a chamber filled with solvent vapor. Depending on the waiting time before introducing the sample, the atmosphere will be more or less saturated with vapor. Moreover, depending on the speed at which the samples are introduced, different gradients are produced. We characterized the gradients by making absorption and ellipsometry maps, X-ray diffraction measurements on different loci of a graded sample and photoinduced absorption on homogeneously annealed samples. Then we characterize the spectral response as a function of position on devices based on P3HT crystallinity gradients along the active layer. We demonstrate that these devices can operate as PSDs under two different detection schemes: monitoring either the absolute photocurrent at one wavelength or a photocurrent ratio at two wavelengths. PSDs operating over 20 mm in length with position determination error below 500 µm are demonstrated. Then we turn to show the potential of this technique for the efficient optimization of solar cells by producing five samples that explore the two time parameters involved in the annealing process, waiting time before introducing the sample into the chamber (related to the degree of vapor saturation in the inner atmosphere) and sample speed. These five graded samples would be equivalent to preparing roughly 100 homogeneous samples with different annealing conditions. Finally, to show the potential of the technique with respect to exploring the capabilities of a given annealing protocol, graded samples are fabricated by gradual vapor annealing using eight different solvents. On the one hand, this helps to identify the relevant parameters for vapor annealing, and on the other, offers a fast route for the screening of good and bad solvents based on just eight samples (c.f. over hundred samples in conventional testing protocols).

## 2. Experimental

### Active layer and device preparation.

In order to create the largest possible gradient, we first explored the deposition conditions for obtaining the P3HT:PCBM layers exhibiting a very low degree of crystallinity. Using absorption measurements as an indirect

technique to evaluate crystallinity (see below), we estimated that the two most relevant parameters for obtaining highly amorphous starting films are the compound concentration in solution, the temperature of the solution during spin coating and, to a lesser extend, other parameters such as the specific spin coating conditions (1000-3000 rpm), the stirring time (4 h to 18 h) and the approximate substrate temperature prior to spin coating (from 0 to 60 °C). Unless otherwise stated, the blend layers discussed hereafter were spin coated at 2000 rpm for 90 s from a 1:1 P3HT:PCBM weight ratio solution (45-50 mg/mL in chlorobenzene, CB) that were kept at 60 °C. The solutions had been stirring for a minimum of 4 h at 50 °C. 96% regioregular-P3HT (Rieke Metals), PCBM (Sigma-Aldrich) and CB (Sigma-Aldrich) were used as delivered. Typical thicknesses of the organic layers were around 200 nm as measured with ellipsometry.

Three types of substrates were employed, namely glass for ellipsometry and absorption; quartz for photoinduced absorption; and patterned ITO-coated glass (purchased from Psiotec, Ltd) for devices and additional absorption and X-ray measurements. The substrates were cleaned with soap water and successively ultrasonicated in acetone (15 min) and isopropanol (15 min). For devices, after nitrogen drying, the anode was UV-$O_3$ treated for 10 min. A 0.2 µm PVDF filtered poly(3,4-ethylenedioxythiophene): poly(styrenesulfonate) (PEDOT:PSS) (Pjet HC from H.C. Starck) solution was spin coated on top of the ITO at 1500 rpm for 90 s and then thermally annealed for 15 min at 90°C in a fume cabinet, producing a ca. 40 nm thick layer. LiF/Al electrodes were thermally evaporated at a base pressure of $9{\cdot}10^{-7}$ mbar through a shadow mask, defining an active area of $5{\times}20$ mm$^2$. Finally, the devices were encapsulated with a glass cap using an ultraviolet curing epoxy resin (Loctite 358). The 5 min exposure to the 90 mW/cm$^2$ UV radiation was performed from the Al metal side in order to avoid photodegradation of the organic layers at the active region.

### Gradient formation.

In order to evaluate the range of vapor exposure times that lead to changes in morphology, we have first measured in-situ reflectivity and transmission experiments during vapor annealing. Depending on the container size and the effective surface of the solvent, variations were observed starting from some tens up to hundreds of seconds. After the initial strong effect of the solvent vapor, a saturation regime is reached, in which the morphology changes considerably slower. The first regime is here selected to create large morphological gradients, and comprise exposure times ranging between 0 s and 400 s. The gradual morphology changes are obtained following three simple steps (see Figs. 1 and 9): 1) a recipient with two small containers filled with solvent is left closed during a fixed time, referred hereafter as waiting time. 2) The sample is introduced through a small gap on the side of the recipient using a step motor with controlled speed. 3) When the whole sample is inside, the recipient is opened and the sample rapidly removed using the same motor (this process takes less than 3 seconds). Alternatively, the sequence of steps can be inverted, starting with the sample inside the recipient and gradually removing it after some waiting time (Fig. 9). As we discuss below, this second approach might be more adequate for organic solar cell optimization, while the first will be better for position sensitive photodetectors in order to create the largest possible gradient. We note that the solvent recipients used for both types of experiments were different. Important aspects to take into account in order to ensure reproducibility include lateral and morphological homogeneity of the as spun sample, tightness degree of enclosure, initial sample position and solvent surface area and depth within its containers.

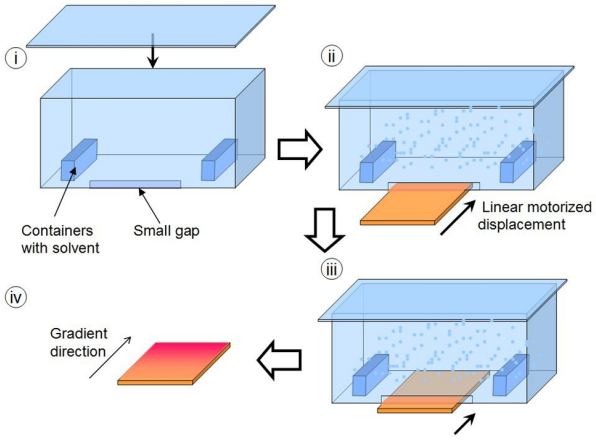


***Fig 1.*** Schematics of the fabrication process: (i) a recipient with two containers filled with solvent is closed and the inner atmosphere is left to saturate. Then (ii) the sample is gradually introduced using a linear step motor at a given speed until the whole sample is inside the recipient (iii). The sample is finally rapidly removed from the container. As a result of the different vapor exposure time at the different points of the sample, a gradient in morphology is generated (iv).

### Device characterization.

The external quantum efficiency (EQE) of the devices was mapped by scanning a focused light beam across the surface of the device. For this, white light coming from an arc lamp source (Hamamatsu 75 W Xe lamp with Oriel Instruments Model 7340 casing and Newport 69907 power supply) is passed through an spectrometer (MicroHR from Horiba Jobin-Yvon, 140 mm focal length) and focused using mirrors and lenses on the sample (spot size was ca 500 µm). A linear motorized stage (THORLABS

MTS25/M-Z8E) moves the sample and the corresponding photocurrent is measured at 1000 µm intervals using a Keithley 2400 Sourcemeter under ambient conditions. The intensity of the incoming light is continuously monitored using a beam splitter and a calibrated THORLABS PM100A photodetector.

### Photometry and ellipsometry.

Polarized transmission, reflection and variable angle spectroscopic ellipsometry (VASE) were performed using a SOPRA GES5E rotating polarizer ellipsometer (SEMILAB) with built-in CCD detection on P3HT:PCBM films deposited on glass and on glass/ITO/PEDOT substrates. Transmission and VASE maps were performed on several graded samples. A confocal objective allowed focusing the incident light beam into a spot about 250 µm wide (in the short direction of the elliptical projection for non-normal experiments). From the transmission data, the Beer-Lambert law was employed to estimate the absorption as a function of position. For the analysis of the VASE data, a number of models were used. These include homogeneous blends, vertical segregated blends, films with surface roughness, and ternary blends of regioregular P3HT, regiorandom P3HT, and PCBM. The reference optical constants were obtained from the literature [17]. The latter was the model that led to the lower fitting standard deviation and showed good convergence (relatively large variations in the initial conditions yielded the same results). The sum of square residuals was further reduced by half when including vertical segregation in a simplified manner [18]: mathematically modeling the film as two sublayers with different blend compositions. The Bruggeman effective medium approximation was used for the optical constants of the binary and effective ternary blends.

### X-rays.

X-ray measurements were performed using a D8Advance diffractometer coupled to a bidimensional Histar detector (that uses a general Area Detector Diffraction System, GADDS). The approximately 1 mm spot size (in the short direction) was scanned along the graded P3HT:PCBM films on top of glass/ITO/PEDOT:PSS substrates and data were collected during one hour at each position, with 2θ varying from 2.5° to 37.5° and a 0.5 mm collimator.

### Continuous wave photoinduced absorption (PIA).

Excitation was provided by a solid state 532 nm diode pumped laser (Roithner LaserTechnik GmbH) with a maximum output power of 100 mW. The laser beam was mechanically chopped at 476 Hz and attenuated with neutral density filters before focusing on the sample. Continuous probe light was provided by a tungsten halogen lamp filtered with a 1/8 m monochromator (CM110 Spectral Products) equipped with two 600 l/mm gratings for the visible and near-IR spectral ranges respectively. Second order diffraction was subtracted with appropriate long-pass filters. Phase sensitive detection was carried out with a SR830 dual channel lock-in amplifier from Stanford Research Instruments in combination with Si and liquid $N_2$ cooled InSb photodiodes (Teledyne Judson Technologies) for detection of the visible and near-IR part of the spectrum respectively. The sample was enclosed on a CFV Optistat Oxford Instruments cryostat and measurements were performed at 77 K.

## 3. Results and discussion

In order to create a sample with a gradual change in morphology (either a change in the degree of film crystallinity and/or phase separation), we have developed a method based on vapor annealing. The idea is that changes associated to solvent vapor exposure depend on the exposure time until saturation is reached [19]. In one possible configuration, a film is slowly introduced using a linear step motor through a small gap into a container filled with vapor of an organic solvent (a good solvent for the specific organic materials considered) (Fig. 1). When the sample is completely introduced, it is then rapidly removed from the container. In this way, the section of the film that entered first the container will be exposed during longer times to solvent vapor compared to the part of the film that was introduced last, thus producing a gradient of vapor exposure. If the step motor speed is slow enough for the vapor to be able to diffuse into the film, but not too slow as to reach saturation in all points of the sample, then the film will exhibit a gradual change in morphology.

In order to illustrate this, we have gradually exposed a P3HT:PCBM spin coated film to an atmosphere saturated with chlorobenzene vapor. For this system, solvent annealing promotes crystallization of the polymer within the blend, which is often accompanied by a bathochromic shift in the absorption spectrum [19]. The shift in absorption upon annealing can be readily detected by the naked eye through a change in film coloration (Fig. 2 (a)). Films gradually exposed to chlorobenzene vapor show a gradual change in color (Fig. 2 (a), middle), suggesting a continuous change in morphology across the moving direction of the step motor (Fig. 1). A quantitative description of this effect is obtained by mapping the absorption spectra as a function of position within the film (Fig. 2 (b)). The absorption of the film is gradually red shifted when moving the probe from the unexposed side to the strongly exposed side of the blend film. This red shift is accompanied by an increasingly better resolved vibronic structure, including the long wavelength absorption shoulder associated with

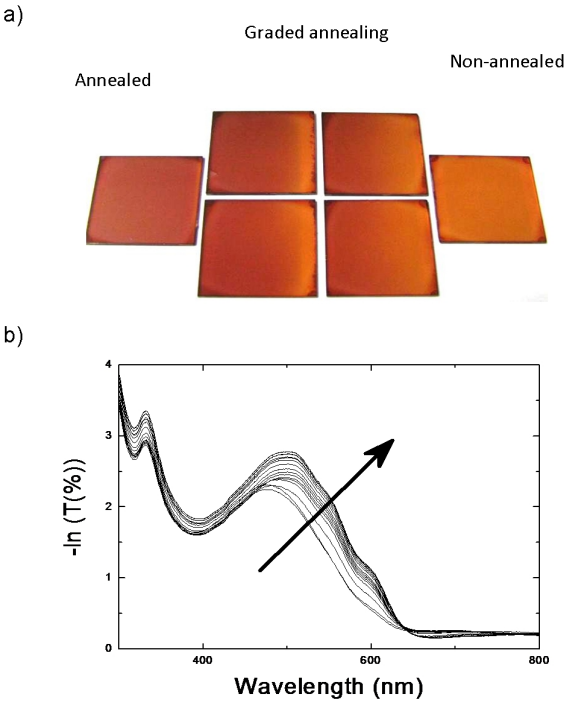


***Fig 2.*** Pictures of homogeneously annealed (left), graded annealed (middle) and non annealed (right) P3HT:PCBM samples. (b) Absorption of a graded film as a function of position. The arrow marks the increase in polymer crystallinity.

high degree of crystallinity [20]. The variation in P3HT crystallinity was also confirmed by variable angle spectroscopic ellipsometry (VASE). VASE data were analyzed using a model consisting of an effective ternary blend of PCBM and semicrystalline and amorphous P3HT. The latter two were modeled with the optical properties of regio-regular and region-random P3HT films, respectively [18]. Figure 3 shows the percentage of amorphous P3HT along the graded film. Note that this does not correspond to the total percentage of amorphous P3HT, as the semicrystalline P3HT (the regio-regular reference) will not be 100% crystalline. In other words, the percentage shown in Fig. 3 would represent the percentage with respect to the pristine regio-regular P3HT reference similarly to what has been recently reported for Raman investigations of molecular order in P3HT:PCBM blends [21]. The ellipsometric map clearly shows the reduction in amorphous polymer fraction for the part of the sample that was exposed to vapor for longer times. Additional details of the ellipsometric analysis can be found in the experimental section and supplementary information (Fig. 10). We have further confirmed the increase in polymer crystallinity by measuring X-ray diffraction at different locations for a graded film deposited on glass/ITO/PEDOT:PSS substrates. A X-ray spot of ca. 1 mm in width allowed to collect several points in the direction of the gradient. Figure 11 shows representative X-ray spectra, demonstrating the enhanced degree of crystallinity along the sample by the clear increase in the (100) diffraction peak of P3HT [20]. Based on the correlation between absorption, ellipsometry and X-ray, hereafter, we will employ the energy position of the absorption maxima and absorption ratio between maxima and shoulder to quantitatively describe crystallinity changes.

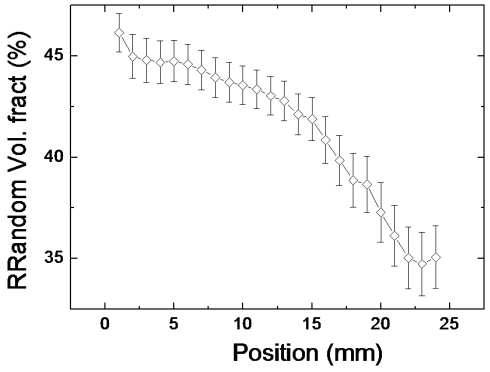


***Fig 3.*** Ellipsometric evaluation of the content of amorphous polymer (modeled as region random P3HT) as a function of position in a graded P3HT:PCBM sample.

Once we have demonstrated that a gradual exposure to solvent vapor can induce a readily detectable increase in crystallinity, we move to the fabrication of photovoltaic devices based on such graded films. For this purpose, we have spin coated films of P3HT:PCBM on top of patterned ITO/ glass substrates coated with a 40 nm thick PEDOT:PSS layer. Then, the gradient was produced following the aforementioned protocol, and finalized by evaporating a 25 mm long LiF/Al top electrode covering the device along the direction of the gradient (see Fig. 12). The devices were encapsulated inside a nitrogen filled glovebox. Figure 4 (a) shows the external quantum efficiency (EQE) measured at regular displacements along the device by focusing the incoming monochromatic beam down to a spot of ca 500 µm in diameter. Following the absorption spectra, the EQE red shifts and the vibronic progression becomes more apparent as the increasingly crystalline part of the active layer is probed [22]. Moreover, since the charge mobility increases with the degree of crystallinity [3], so it does the photocurrent when departing from the more amorphous side of the device towards the more crystalline side (Fig. 4 (b)). This device constitutes a proof of principle for a position sensitive photodetector as the response depends on the specific posi-

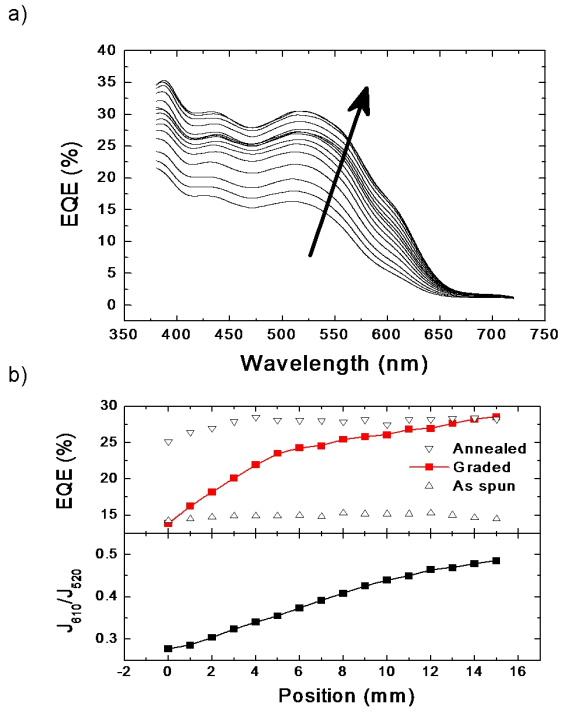


***Fig 4.*** (a) External quantum efficiency as a function of position for a PSD based on a gradual change in P3HT crystallinity. (b) EQE (top) and photocurrent ratio (610/520) for the same PSD. The open triangles correspond to a homogeneously crystallized (down) and non annealed (up) samples.

tion in which light hits the device area. Compared to previous published organic PSDs, this device does not rely on the lateral resistivity of the ITO [11] or on the varying electric field distribution across the devices produced by a lateral gradual change in film thickness [15, 16]. Instead, it is based on the produced gradient in morphology. As a PSD, the advanced device could operate in two modes. One may simply register the absolute value of the photocurrent at a given wavelength (e.g. around the maximum EQE) as shown in Fig. 4 (b) top panel. This mode would require, however, previous knowledge of the intensity of the incoming light beam. To avoid this, one could take advantage of the bathochromic shift produced by the different degree of crystallinity. By performing a ratiometric measurement at two different wavelengths [15] (for instance, at the position of the crystallization shoulder and the maximum of the EQE) a more linear dependence on position is obtained (Fig. 4 (b) bottom). This mode of operating the PSD would not require previous knowledge of the incoming beam intensity but would, on the other hand, be based on the alternated incidence of monochromatic beams centered at two different wavelengths.

The response of the PSD is normally calibrated as a function of position. However, sometimes a linear dependence on position might be preferred [11]. In order to achieve this, further optimization should be undertaken with respect to the fabrication protocol. Three important aspects need to be considered for this. First, the amount of solvent vapor molecules in the chamber does not linearly increase with time, but has a saturation point. Secondly, the crystallization behavior of the polymer exposed to vapor typically follows an Avrami type exponential relationship with time [23]. And finally, the charge mobility (and EQE) does not depend linearly on the degree of crystallization [3]. Therefore, if a given shape for the response as a function of position is desired, these three effects need to be taken into account.

We note that the EQE values for the graded device vary between those of non-annealed films and homogeneously annealed films. This is due to the fact that the solvent vapor was left to (almost) saturate the atmosphere before introducing the film. Alternatively, gradual structures can also be fabricated by closing the lid of the container with the sample inside, and slowly removing the sample from the container through the gap after a waiting time (Fig. 9). This second procedure implies that the less exposed area would still exhibit larger crystallinity than a non-annealed film, simply because of the homogeneous vapor exposition during the waiting time. A lesser crystallinity gradient will be reflected in a lower variation of the EQE along the graded film. Thus the first procedure will be preferred for PSD applications in order to achieve the largest dynamical range possible in position measurement. Conversely, when attempting to optimize the annealing protocol for a solar cell, both sequences of steps may be employed. Here we have used the alternative method for solar cells (the sample already inside the recipient when the lid is closed) as this might result in better reproducibility with standard homogeneously annealing fabrication conditions.

Next, we explored the potential of graded structures for the optimization of solar cells. We have fabricated five graded samples by fixing the stage speed (at 1 cm/min) and varying the waiting time. Note that these two parameters are not equivalent since the container is not hermetically closed (there is a gap through which the sample is introduced or removed from the container). As we are measuring every half millimeter, we estimate that these five samples would be equivalent to about 100 homogeneous samples. Figure 5 shows the maximum EQE values (a) and position of the absorption maximum (b) for samples with different waiting times as a function of position. The degree of crystallinity (evaluated by the position of the maximum in absorption in Fig. 5 (b)) increases with exposure time. Interestingly, the maximum EQE does not

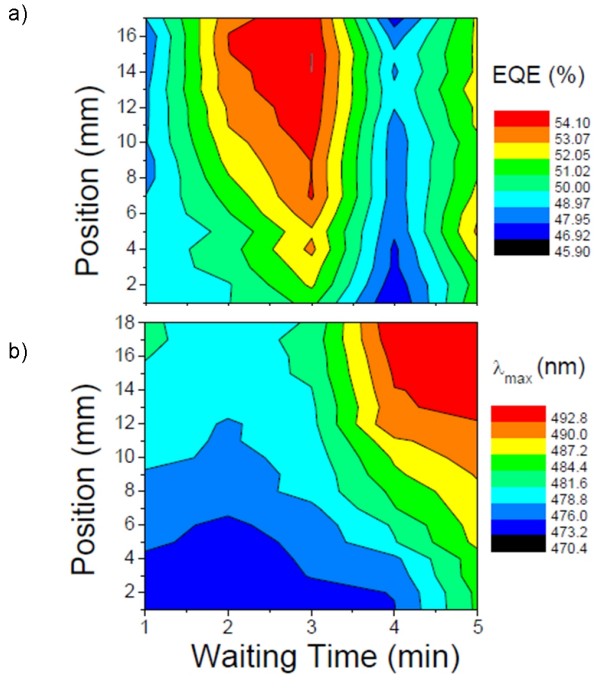


***Fig 5.*** Maximum value of the EQE (a) and wavelength at the absorption maximum (b) for a series of P3HT:PCBM graded devices fabricated with different waiting times.

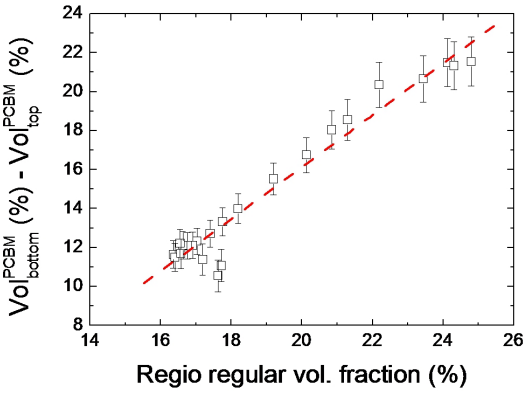


***Fig 6.*** Correlation between the degree of crystallinity (with respect to regio regular P3HT) and the vertical segregation on a graded film (see details of the analysis in the experimental section). If all the P3HT chains were as crystalline as the pristine regio regular P3HT, and considering that these are 1:1 P3HT:PCBM mixtures, the volume fraction would be 50%.

follow the same trend. A maximum EQE value was obtained for waiting times of 3 minutes on samples that were exposed the longest times, *i.e.* effective accumulated exposure time of about 4 minutes. Samples exposed over longer periods of time did show an increase in crystallinity, but, however, led to a worsening in photovoltaic performance. We argue that this is due to an excessively large degree of phase separation [18]. This hypothesis is supported by the ellipsometric analysis of data collected for graded samples on glass. Figure 6 shows the almost linear relationship that we obtained for the degree of vertical phase separation (see experimental section) and the degree of film crystallinity. In other words, increasing the polymer crystallinity also leads to a more pronounced phase separation. A large degree of phase separation would reduce the charge transfer probability and thus the generated photocurrent. To further prove this idea we have performed PIA experiments on four samples vapor annealed during different times, namely 0 s, 120 s, 240 s and 600 s. (Note that as the recipient for vapor annealing was different, direct comparison of times cannot be made). Figure 7(a) displays the PIA spectrum of a vapor annealed blend. The spectrum, in agreement with previous findings, is characterized by two absorption peaks corresponding to the two symmetry allowed P3HT polaron transitions located at 1.2 eV (P2) and 0.5 eV (P1). On account of the non negligible out-of-phase component and the modulation frequency (470 Hz), we infer that a large percentage of polarons recombine in timescales exceeding 1 ms. A comparison of $\Delta T/T$ module for the four different samples indicates a clear enhancement in polaron population with crystallinity except for the highest crystalline sample where a clear signal drop is found. Such dependence must be attributed to a gradual increase in charge photogeneration efficiency as the crystallinity increases. Note that the similar de-phasing angle found for the four samples (1.58 $\pi$– 1.89 $\pi$ rad) rules out strong changes in recombination behavior as an alternative explanation for the observed $\Delta T/T$ dependence with crystallinity. The low charge photogeneration yield in the more crystalline sample is consistent with the observed drop in EQE. Finally, we show another example of the wide potential of this technique for the optimization of annealing protocols as well as providing fundamental insights with respect to the mechanisms of crystallization upon vapor annealing. For this, we have fabricated graded samples keeping the motor speed (0.07 mm/s) and waiting time (60 seconds) constant and varying the solvent used in vapor annealing. We have tested chlorobenzene, o-dichlorobenzene, 1,2,4-trichlorobenzene, chloroform, p-xylene, toluene, tetrahydronaphtalene, and hexane. In order to evaluate how efficiently the different solvents can promote crystallization in P3HT:PCBM blends, we use the ratio of the absorption at the crystallization shoulder (600 nm) and the maximum of absorption, which, as already discussed, increases with crystallization (see above

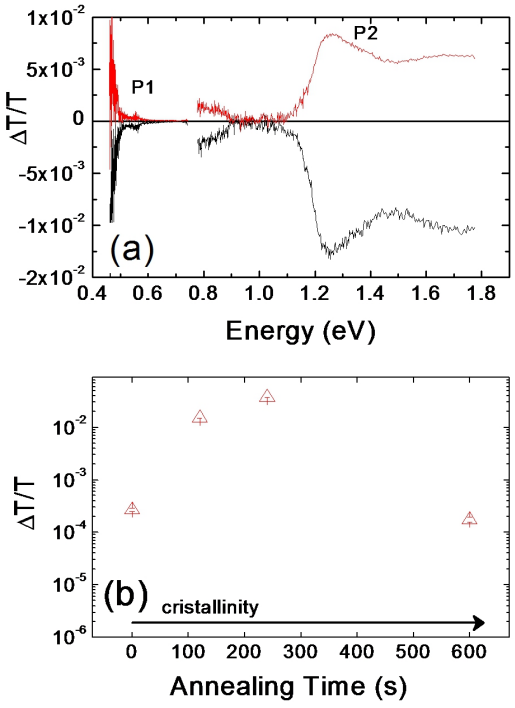


***Fig 7.*** (a) CW-PIA spectra for a vapor annealed P3HT:PCBM bulk heterojunction film deposited on quartz. (b) Evolution of the P2 peak intensity as a function of vapor annealing time.

and ref [20]). Figure 8(a) shows this ratio as a function of position (closer to 20 mm corresponds to longer exposure times) ordering the solvents with increasing crystallization potential (see also Fig. 14(a)). A linear interpolation has been performed between solvents in order to simulate potential results of solvent mixtures. The first observation is that most of the solvents produced gradients in crystallinity with p-xylene producing the highest crystallization ratio (0.51) and hexane the minimum (ca. 0.10). These eight graded samples enable a rapid evaluation of the different solvents and understanding what are the relevant parameters for producing a rapid crystallization of P3HT. The first intuitive mechanism would be the number of solvent vapor particles in the container atmosphere, something that could be parameterized by looking at the boiling point (Figs. 8 (c) and 14) and/or the vapor pressure (Fig. 8 (d)). We notice that when including the eight different solvents, none of these two parameters produce a single maximum (in fact they show three), suggesting that the relationship between solvent properties and degree of crystallization is more complex. When attending only to chlorinated solvents (Fig. 14 (b)), we can conclude that the higher the boiling point, the lower the degree of crystallization achieved for a given exposure time.

Another observation is that hexane seems to have a very small effect on crystallinity. As hexane is a particularly bad solvent for P3HT and PCBM, we investigated how the solubility affects the final degree of crystallinity. For this, we evaluated the Hansen solubility parameters, which accounts for dispersion forces, intermolecular interactions and hydrogen bonding. The dispersive components of the Hansen solubility parameters are shown in Figure 8 (b) for the different solvents. A clear maximum is observed in this disposition. Looking closely at the Hansen parameters for both components, it appears that the higher crystallinity is achieved when the solvent is a good solvent for both donor and acceptor molecules, but relatively better for the polymer (Fig. 15). Hence, solubility of the materials on the solvent is one of the most important solvent parameters for an effective solvent annealing process. Other parameters, such as solvent density, viscosity and surface tension may also play a role, but they do not seem to be the most relevant factors determining the final degree of crystallization (Fig. 16). To sum up this part of the results, probably a combination of boiling point and solubility are the two major parameters that determine how good a solvent is in order to promote polymer crystallization (Fig. 16 (h)).

## 4. Conclusions

We have developed a simple technique to produce blend films with a controlled lateral gradient in morphology. When sandwiched between a PEDOT coated ITO transparent anode and LiF/Al cathode, this graded layer constitutes the basis of a position sensitive photodetector based on a radically different concept that the existing ones: different morphologies give different spectral photoresponse at different positions. Moreover, this type of graded samples can be utilized to optimize organic solar cells, and their annealing protocols. We show how this can be done for P3HT:PCBM based photovoltaics and also demonstrate that excessive annealing may lead to a too large degree of phase separation and thus lower photocurrent. Finally, graded films are employed as a proof of principle screening technique for solvents employed during solvent annealing.

## Acknowledgements

The authors thank the Spanish Ministerio de Economía y Competitividad for funding through the projects MAT2009-10642, PLE2009-0086, MAT2012-37776, and TEC2010-21830-C02-02 as well as Ramon y Cajal contract number RYC-2009-05475. We are indebted to Ignasi Burgués (ICMAB) for assistance with evaporation and encapsulation, to Anna Crespi (ICMAB) for assistance with

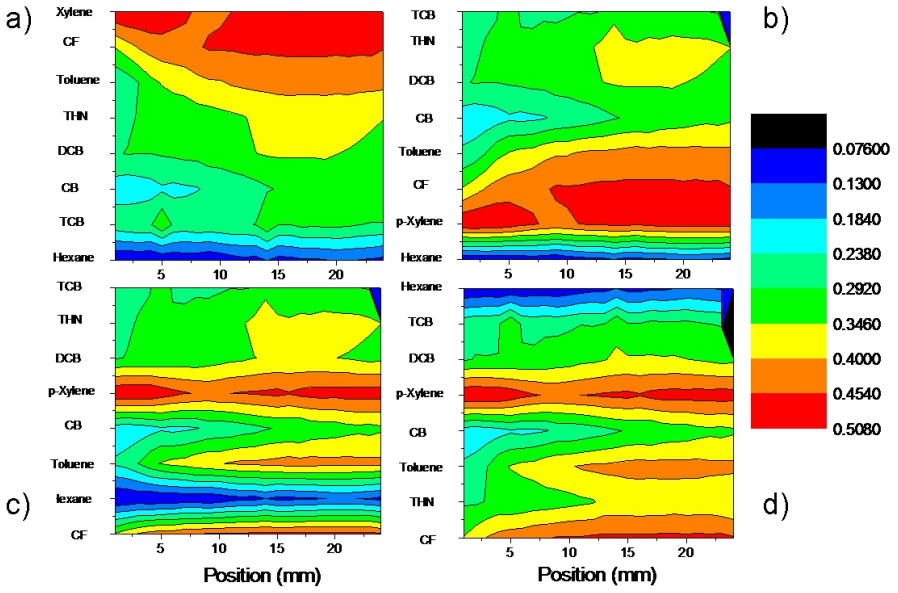


***Fig 8.*** Relative absorption between the crystallinity shoulder (600 nm) and the maximum of absorption as a function of different solvents. The x axis shows the position in the graded film while the solvents are ordered in the Y axis according to (a) maximum crystallinity achieved, (b) the Hansen parameters, (c) the boiling point, and (d) the vapor pressure.

the X-ray measurements, to Dmitri Nassyrov (ICMAB) for his help at the early stages of this project, and to M.I. Alonso and A. Goñi (ICMAB) for fruitful discussions. We also acknowledge PCT patent with application number PCT/ES2011/070841 and publication reference WO/2012/076740.

## References

[1] D. Chirvase, J. Parisi, J. C. Hummelen, V. Dyakonov, Nanotech., 15, 1317 (2004).
[2] F. Padinger, R. S. Rittberger, and N. S. Sariciftci, Adv. Funct. Mater., 13, 85 (2003).
[3] V. D. Mihailetchi, H. Xie, B. de Boer, L. J. A. Koster, P. W. M. Blom, Adv. Funct. Mater., 16, 699 (2006).
[4] T. Agostinelli, M. Campoy-Quiles, J. C. Blakesley, R. Speller, D. D. C. Bradley, J. Nelson, Appl. Phys. Lett., 93, 203305 (2008).
[5] Y. Kim, S. A. Choulis, J. Nelson, D. D. C. Bradley, S. Cook, J. R. Durrant, J. Mater. Sci., 40, 1371 (2005).
[6] G. Li, Y. Yao, H. Yang, V. Shrotriya, G. Yang, Y. Yang, Adv. Funct. Mater., 17, 1636 (2007).
[7] J. Cabanillas-González, J. Nelson, D. D. C. Bradley, M. Ariu, D. G. Lidzey, D. D. C. Bradley, Synth. Met., 137, 1471 (2003).
[8] G. Li, V. Shrotriya, J. Huang, Y. Yao, T. Moriarty, K. Emery, Y. Yang, Nat. Mater., 4, 864 (2005).
[9] J. Peet, J. Y. Kim, N. E. Coates, W. L. Ma, D. Moses, A. J. Heeger, G. Bazan, Nat. Mater., 6, 497 (2007).
[10] L. Hou, E. Wang, J. Bergqvist, B. V. Andersson, Z. Wang,C. Müller, M. Campoy-Quiles, M. R. Andersson, F. Zhang, O. Inganäs, Adv. Funct. Mater., 21, 3169 (2011).
[11] B. P. Rand, J. Xue, M. Lange, S. R. Forrest, IEEE Phot. Tech. Lett., 15, 1279 (2003).
[12] D. Kabra, Th. B. Singh, K. S. Narayan, Appl. Phys. Lett., 85, 7073 (2004).
[13] R. Koeppe, P. Bartu, S. Bauer, N. S. Sariciftci, Adv. Mater., 21, 3510 (2009).
[14] J. Cabanillas-González, M. Campoy-Quiles, PCT patent application PCT/ES2011/070841.
[15] J. Cabanillas-González, O. Peña-Rodriguez, I. S. Lopez, M. Schmidt, M. I. Alonso, A. R. Goñi, M. Campoy-Quiles, Appl. Phys. Lett., 99, 103305 (2011).
[16] J. Cabanillas-González, M. Schmidt, O. Peña–Rodríguez, M. I. Alonso, A. R. Goñi, M. Campoy-Quiles, J. Nanosci. Nanotechnol., 13, 5158 (2013).
[17] M. Campoy-Quiles, J. Nelson, D. D. C. Bradley, P. G. Etchegoin, Phys. Rev. B, 76, 235206 (2007).
[18] I. Burgués-Ceballos, M. Campoy-Quiles, L. Francesch, P. D. Lacharmoise, J. Polym. Scien. Part B: Poly. Phys., 50, 1245 (2012).

[19] M. Campoy-Quiles, M. Schmidt, D. Nassyrov, O. Peña, A.R. Goñi, M.I. Alonso, M. Garriga, Thin Solid Films, 519, 2678 (2011).
[20] T. Erb, U. Zhokhavets, G. Gobsch, S. Raleva, B. Stühn, P. Schilinsky, C. Waldauf, C. Brabec, Adv. Funct. Mater., 15, 1193 (2005).
[21] W. C. Tsoi, D. T. James, J. S. Kim, P. G. Nicholson, C. E. Murphy, D. D. C. Bradley, J. Nelson, J.-S. Kim, J. Am. Chem. Soc., 133, 9834 (2011).
[22] J. Clark, J.-F. Chang, F. C. Spano, R. H. Friend, C. Silva, Appl. Phys. Lett., 94, 163306 (2009).
[23] D. Nassyrov, C. Müller, A. Roigé, I. Burgués-Ceballos, O. J. Ossó, D. B. Amabilino, M. Garriga, M. I. Alonso, A. R. Goñi, M. Campoy-Quiles, J. Mater. Chem., 22, 4519 (2012).

## CONTINUOUS LATERAL GRADIENTS IN FILM MORPHOLOGY FOR POSITION SENSITIVE DETECTION AND ORGANIC SOLAR CELL OPTIMIZATION

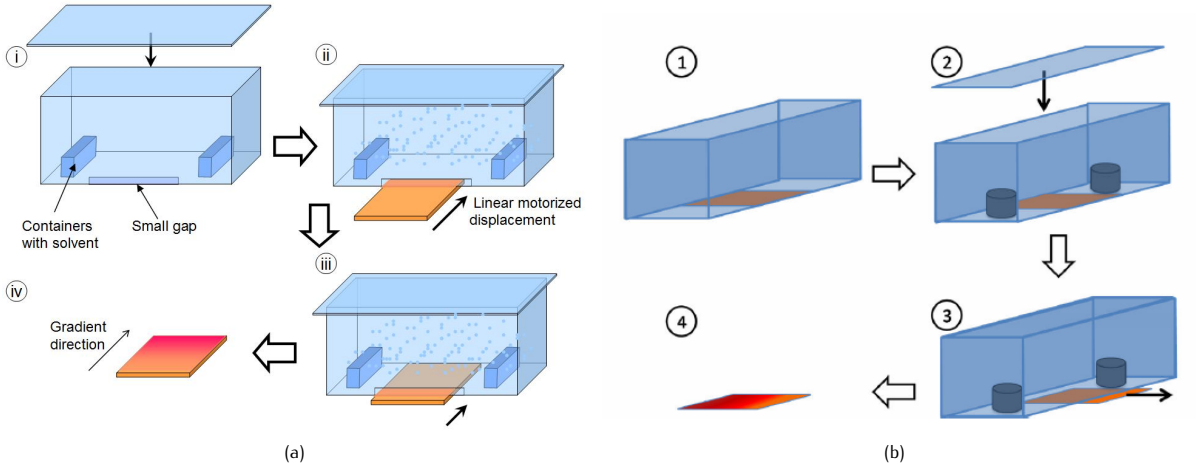


***Fig 9.*** Two modes for the fabrication of gradients: (a) letting the atmosphere saturate first and then introducing the sample, and (b) having the sample inside of the recipient from the beginning and gradually removing the sample after a given waiting time inside.

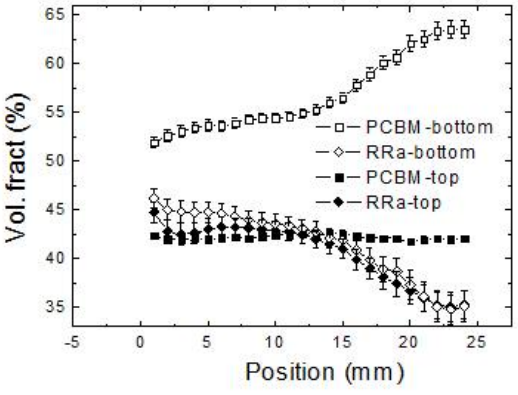


***Fig 10.*** Ellipsometric analysis of a graded film on glass. The model consisted of a bilayer with different amounts of amorphous (regio random), semicrystalline (regio regular) P3HT and PCBM. It can be observed how the regio random P3HT content decreases with increasing vapor exposure time, and, on the other hand, how the vertical segregation (PCBM distribution) increases when crystallizing the film.

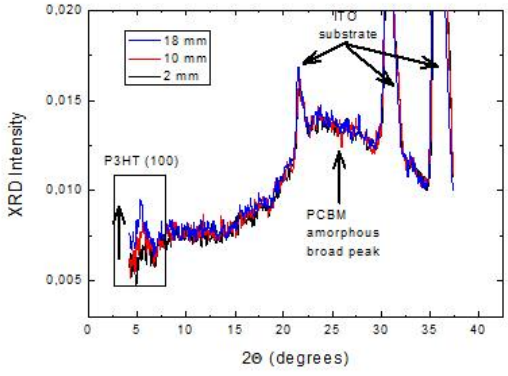


***Fig 11.*** XRD data taken at different positions on a graded film with a 1 mm wide X-ray spot. The increase in the (100) P3HT peak, suggesting increased crystallinity, is apparent from these data.

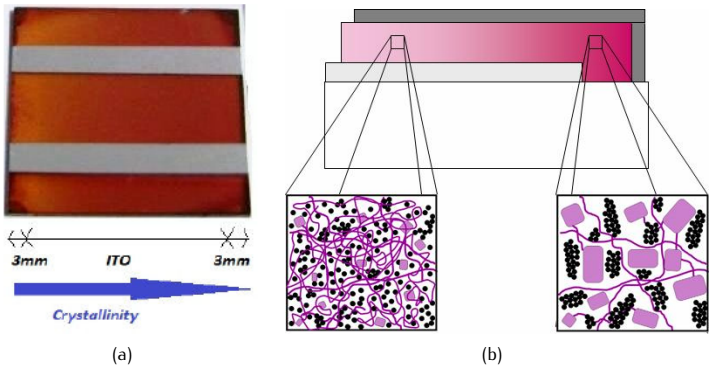


***Fig 12.*** (a) Picture of a device consisting of a P3HT:PCBM layer exhibiting a gradient in morphology sandwiched between electric contacts and (b) diagram of the morphology.

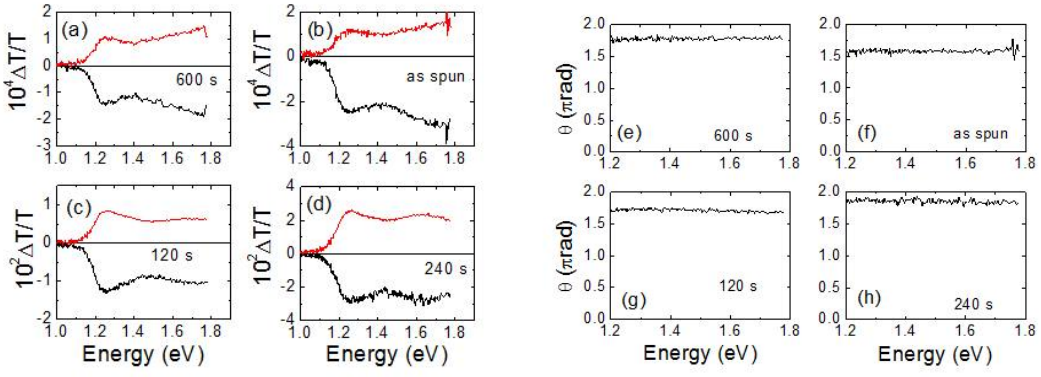


***Fig 13.*** (a)-(d) In phase (black) and out of phase (red) PIA components for samples with annealed during different times (0, 120, 240 and 600 s, as indicated). (e) – (h) PIA phase angle for all samples as a function of energy.

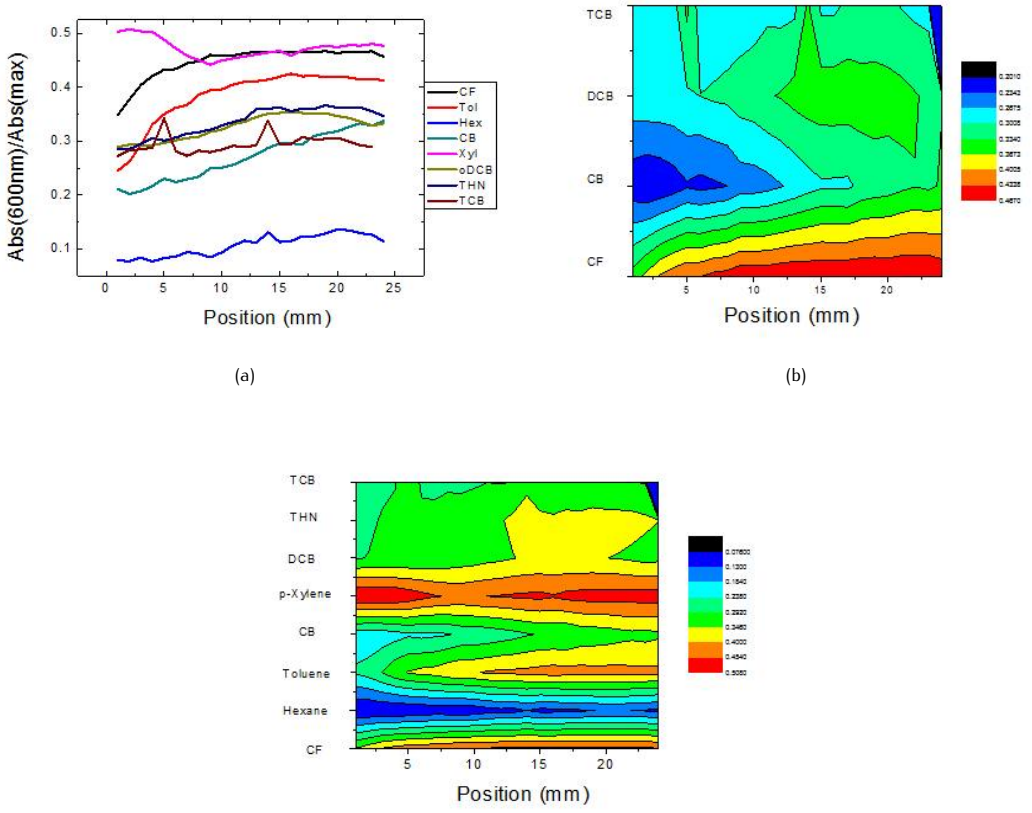


***Fig 14.*** (a) Ratio of the absorption at 600 nm with respect to the absorption maximum as a function of position within the graded film (closer to 20 mm corresponds to longer exposure times). (b) The same ratio plotted as 2D maps with interpolated values ordered by boiling point for the chlorinated solvents (b) and for all considered solvents (c).

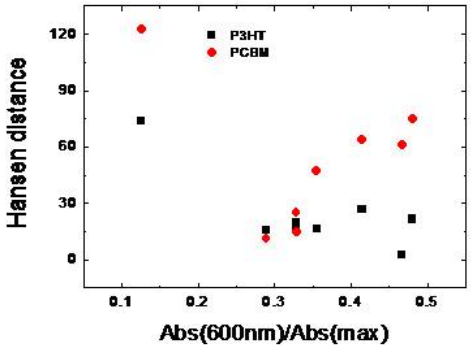


***Fig 15.*** The distance in the Hansen parameter space for the different solvents and the two types of molecules as a function of the absorption ratio at the crystallinity shoulder and the maximum (the crystallinity increases with moving to larger X values).

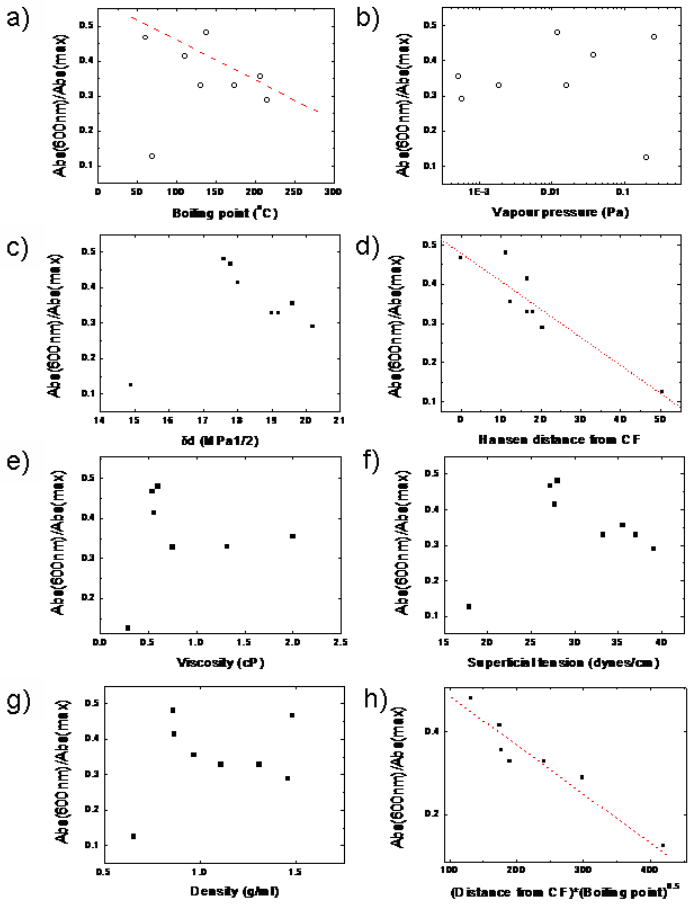


***Fig 16.*** Maximum crystallinity achieved as a function of solvent characteristics: (a) boiling point; (b) vapour pressure; (c) Hansen dispersion parameter; (d) Hansen distance to CF; (e) viscosity; (f) Superficial tension; (g) density; (h) product of the Hansen distance from CF and the square root of the boiling point.